Mechano-electronic Superlattices in Silicon Nanoribbons

Minghuang Huang,[†] Clark S. Ritz,[‡] Bozidar Novakovic,[§] Decai Yu,[∥] Yu Zhang,[∥] Frank Flack,[†] Donald E. Savage,[†] Paul G. Evans,[†] Irena Knezevic,[§] Feng Liu,[∥] and Max G. Lagally[†,‡,*]

[†]Department of Materials Science and Engineering, [‡]Department of Physics, and [§]Department of Electrical and Computer Engineering, University of Wisconsin, Madison, Wisconsin 53706, and [∥]Department of Materials Science and Engineering, University of Utah, Salt Lake City, Utah 84112

ABSTRACT Significant new mechanical and electronic phenomena can arise in single-crystal semiconductors when their thickness reaches nanometer dimensions, where the two surfaces of the crystal are physically close enough to each other that what happens at one surface influences what happens at the other. We show experimentally that, in silicon nanomembranes, through-membrane elastic interactions cause the double-sided ordering of epitaxially grown nanostressors that locally and periodically highly strains the membrane, leading to a strain lattice. Because strain influences band structure, we create a periodic band gap modulation, up to 20% of the band gap, effectively an electronic superlattice. Our calculations demonstrate that discrete minibands can form in the potential wells of an electronic superlattice generated by Ge nanostressors on a sufficiently thin Si(001) nanomembrane at the temperature of 77 K. We predict that it is possible to observe discrete minibands in Si nanoribbons at room temperature if nanostressors of a different material are grown.

KEYWORDS: silicon nanomembrane · Ge quantum dots · strain superlattice · minibands · Seebeck coefficient

Single-crystal silicon membranes with nanometer thicknesses have mechanical properties that can be exploited to produce unique structural and electronic effects. Their mechanical compliance makes membranes fundamentally different from bulk materials or supported thin films.[1,2] The growth of nanostressors on ultrathin Si membranes takes advantage of this mechanical compliance to create a "strain lattice" consisting of very small regions of high local strain in the membrane, the order occurring because the local strain provides a strong and precise feedback for self-organization of the nanostressors. The strain lattice in the Si membrane in turn produces a modulation in the electronic band structure that extends through the thickness of the membrane and thus creates an electronic superlattice without a need for compositional modulation, the conventional method for forming electronic heterostructures. The ability to create straightforwardly such functional superlattices in semiconductors has significant implications for the development of nanoscale photonic, electronic, and thermoelectronic devices. The mechanism should be accessible in membranes of all the semiconductor systems that exhibit strain-mediated growth of nanostructures.

Ultrathin Si nanomembranes, created by thinning and releasing a single-crystal Si sheet, such as the outer Si layer (template layer) of silicon-on-insulator (SOI), extend the use of Si to many new applications.[3−5] These Si nanomembranes can be completely free-standing or partially attached to a substrate, and either flat or curled into hybrid three-, two-, or one-dimensional structures.[6,7] The membranes can be patterned into free-standing ribbons or wires of any shape or orientation,[6,7] limited only by nanolithography techniques. What distinguishes any of these crystalline structures in membrane form from thick, rigid materials is that the two surfaces of the membrane are physically close enough to each other that what happens on one surface influences what happens on the other. In particular, processes depending on elastic interactions are completely changed by accessibility to both membrane surfaces and the ability of the membrane to respond by changing its shape and dimensions.

We have fabricated membranes and ribbons from SOI on which the Si template layer is thinned by successive oxidation and chemical etching to leave a Si sheet with 5−50 nm thickness on a buried layer of SiO_2. Etching away the underlying oxide layer makes the membranes free-standing. In the work reported here, we pattern the Si template layer to obtain free-standing (*i.e.*, accessible on all sides) nanoribbons that remain attached at both ends to the Si handle wafer and buried oxide. The nanoribbons are typically 50−250 nm wide.

See the accompanying Perspective by Kim and Rogers on p 498.

*Address correspondence to lagally@engr.wisc.edu.

Received for review December 22, 2008 and accepted January 26, 2009.

Published online February 11, 2009.
10.1021/nn8008883 CCC: $40.75

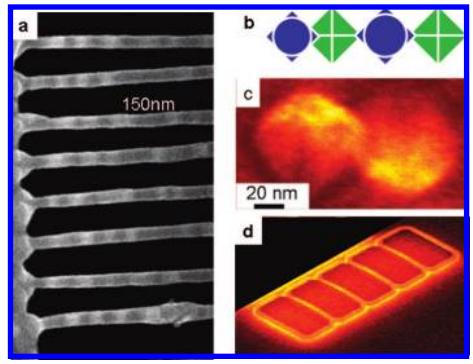

Figure 1. Nanostressors on Si nanoribbons. (a) Scanning electron micrograph of rows of pure Ge QDs on ~20 nm thick, ~80 nm wide Si(001) nanoribbons cut along [110] and tethered on both ends. The order is evident. The dots on each surface are separated by ~150 nm. (b) Schematic diagram of dot ordering on the two surfaces of the ribbon. (c) Relationship between nucleation on top and bottom of a ribbon; 8 nm high, 80 nm base width Ge QDs, on top (left) and on the bottom (right). The Si ribbon is sufficiently thin so that a scanning electron microscope images both sides simultaneously. When the electron beam is incident on the sample at a large angle with respect to the surface normal, the geometric projection of Ge QDs on the top (at left) and bottom (at right) of a Si membrane is different and the two types of QDs can be distinguished. (d) SEM micrograph of a set of nanoribbons showing global bending.

Ge or a Ge-rich SiGe alloy is deposited simultaneously on both sides of these free-standing nanoribbons using chemical vapor deposition (CVD). Because CVD involves the vapor phase transport of precursor molecules, deposition is possible at all locations accessible to the growth gases. Pyramid-shaped strained nanocrystals ("hut" quantum dots[8] (QDs)) form on the two ribbon surfaces *via* the Stranski−Krastanov growth mode.[9] Simultaneously growing nanostressor QDs on both surfaces of an ultrathin Si membrane allows the strain fields of QDs to interact across the thickness of the membrane. Ordering of the QDs occurs because the locally distorting thin ribbon provides a strong and precise feedback for self-organization of the nanostressors. The important result is a periodically strained (primarily *via* bending rather than stretching) thin single-crystal Si ribbon. As we show below, this periodic strain creates an electronic band gap periodicity on the 50−100 nm lateral scale, in effect a *mechano-electronic superlattice*. Whereas these results are novel, to show that they are physically interesting, we must demonstrate two things: that the strain is high enough to induce a meaningfully large change in the band gap, and that we have a superlattice.

RESULTS AND DISCUSSION

Figure 1 shows examples of structures produced by depositing Ge or SiGe on both sides of free-standing but end-tethered nanoribbons with (001) surfaces formed from ultrathin SOI(001). Growth on nanoribbons produces one or more lines of QDs, depending on the width of the ribbon, on both the top and the bottom surfaces of the ribbon. The QDs on the two surfaces of the ribbon assemble in a highly ordered lattice, as shown schematically in Figure 1b, which is square if two or more rows of dots form.[10] The QDs on each surface are aligned in rows along the <100> elastically soft crystallographic directions of Si, but those on one surface are offset in the <100> direction from those on the other surface. This offset is shown in Figure 1c, an SEM image of an 8 nm high, pyramidal QD on the top surface (left) and one on the bottom surface (right). The size and separation of the QDs depends on the QD composition, with both size and separation larger if the QD is SiGe alloy, rather than pure Ge. The alignment and offset are understood in terms of the anisotropic elastic constants of Si[10] and are independent of the crystallographic direction in which the ribbon is cut.

All prior examples of QD growth and ordering to our knowledge involve bulk rigid substrates. In these situations, the significant local strain caused by the nanostressor is shared between the nanostressor and an effectively infinitely thick substrate, while for a nanomembrane it is shared between the nanostressor and a very thin sheet. It is physically intuitive and experimentally and theoretically shown[4,11,12] that strain is much more effectively transferred to the thin sheet. A large local strain in the substrate can occur only when it is thinned down to the nanometer scale, one of the conditions we require. The strain is greater for higher Ge concentration in the QD, and the strain transfer is greater the thinner the Si membrane is.

Our second requirement is the order. How does nanostressor ordering occur on a membrane? Ordered arrays of QDs are themselves not new.[13] It is known that a high degree of order can be induced in arrays of QDs grown on bulk substrates by controlling their nucleation in multiple-layer growth,[14,15] in a single layer spatially confined on a nanopatterned ridge or mesa,[16] or in a single layer at regions in microstructures that have the appropriate curvature, *via* chemical-potential control.[17] All these results are on bulk rigid substrates. For thin membranes, the strain field induced by a nanostressor on one side reaches all the way through the thin sheet. The through-membrane elastic interactions cause interactive and coordinated QD ordering on the two sides of the ribbon that is mediated by the elastic constants of the material.[10] The ordering rivals that on patterned bulk material[16,17] and is much better than single-layer ordering on extended bulk surfaces.[18]

For nanostressor growth on a double-tethered ribbon, there is additionally a global response of the ribbon—once many QDs have formed on the ribbon, the overall effect of the QDs is like that of a continuous compressively strained film on both surfaces of the ribbon,[11] and the ribbon must get longer. The behavior is the same as in the strained-nanomembrane sandwiches described elsewhere,[4] except that here the ribbon is

constrained and thus must bow, randomly "up" or "down" (Figure 1d). Experimental details of the nanostressor ordering on thin membranes will be presented elsewhere.[18]

The electronic properties (band structure, transport) of semiconductors are significantly influenced by strain. As just discussed, the membrane geometry, *via* its thinness and high mechanical compliance, allows the transfer of a high degree of strain,[4] and hence electronic effects in Si associated with lattice strain[19] from a given stressor will be much more evident in thin single-crystal ribbons or membranes than in bulk substrates, where they are effectively negligible. Translated to arrays of nanostressors on ribbons, it means we create a periodic strain field in Si that is high enough to cause significant local band gap variations, something that cannot occur in bulk substrates and is unique to very thin substrates.

Lattice strain alters the valence and conduction bands of Si by shifting them in energy, distorting them, and removing degeneracy.[20] For Si(001), the six degenerate conduction band minima along the <100> axes split into two groups when applying biaxial strain. For biaxial tensile strain, the energy of the two Δ_2 valleys (perpendicular to the (001) plane) is lowered, while that of the four equivalent in-plane Δ_4 valleys is raised. Compressive strain reverses the directions of splitting of Δ_4 and Δ_2.[21] The valence band also shifts with strain, to a lesser degree. The net effect of strain, either compressive or tensile, is to reduce the band gap. A tensile in-plane strain on the order of >1% is readily achievable locally (on the scale of 100 nm) in a Si nanoribbon.

Figure 2a shows the strain dependence of the Si band gap.[22] Using these results, we calculate the periodic change in the Si band gap in the electronic superlattice as a function of position by introducing realistic values of the local strain. We model the local strain with a 2D finite-element analysis of the elastic deformation and elastic energy resulting from two opposite-side QDs in one dimension (Figure 2b) corresponding to the ribbon geometry with one line of dots on each side (Figure 1b) (see Supporting Information).

The strain leads to a significant depression in the band gap of the Si nanoribbon under each QD. The magnitude and period of the band gap minima are influenced by the thickness and crystallographic orientation of the nanoribbon and both the size and composition of the nanostressor. Our calculations, based on the experimental results shown in Figure 1, predict that the maximum tensile strain beneath a pure-Ge "hut" QD with a height of 8 nm and a base width of 80 nm, epitaxially grown on a Si membrane, is 1.62% for a 25 nm thick ribbon and 1.89% for a 10 nm thick ribbon. The resulting reduction of the band gap can be up to 250 meV (Figure 2a), more than 20% of the bulk value of the band gap for the thinnest ribbons.

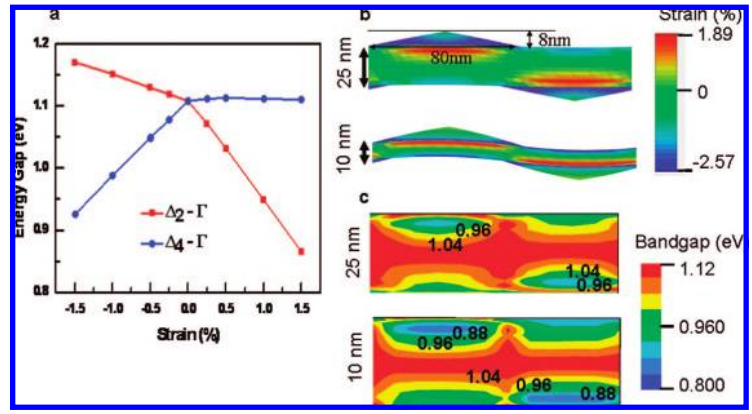

Figure 2. Effect of strain on local band structure of a Si membrane. (a) First-principles calculations of the variation in the Si band gap with biaxial in-plane strain; Δ_4 and Δ_2 are the originally degenerate conduction band valleys in Si, and Γ is the valence band maximum. The gap decreases for both tensile (positive values) and compressive strain (after ref 22). (b) Finite-element analysis of the in-plane component of the strain in a one-dimensional membrane with a QD lattice described by lattice constant L = 160 nm and separation $d = L/2$, matching the measured density of QDs. The calculated strain profiles are shown for both 25 and 10 nm thick membranes. (c) Mapping of the local band gap modulation due to the strain field induced by Ge QDs on both the 25 and 10 nm thick membranes. The band gap ranges from slightly less than the bulk band gap of 1.12 eV in the center of the membrane to approximately 0.95 eV in the region of maximum strain beneath the QDs for the 25 nm thick membrane. The maximum strain beneath a QD on the 10 nm membrane is greater than for the thicker membrane, and therefore the local modification of the band structure is also increased.

It is possible to confirm this band gap modulation experimentally, at least qualitatively. In separate studies on defect-free, flat, uniformly strained Si nanomembranes, we have quantitatively determined the shift of several features in the conduction band structure of Si with increasing tensile strain, using X-ray absorption spectroscopy with secondary electron yield detection. We use ~100 eV transitions from the 2p levels to the conduction band of Si. The limited mean free path of 100 eV or lower-energy electrons assures thin-sheet sensitivity, and tuning to the Si 2p line assures selectivity to Si. The use of synchrotron radiation and a high-resolution monochromator gives 10 meV resolution. Figure 3a shows schematically the shifting of the conduction bands.[19] The total "downward" shift of the conduction band minimum (Δ_2 valleys) at 1% strain is measured to be ~200 meV. [19] This measurement determines only the shift of the conduction band edge: The top of the valence band (Γ point) also moves very slightly with strain. The band gap lowering is a combination of these two shifts. Calculated values of the band gap lowering as a function of position are shown in Figure 2c.

The spatial resolution of XAS in the above form is poor, and thus unsuitable for exploring the spatial variation in band gap. However, by combining photoelectron emission microscopy (PEEM) as the detection tool with high-resolution XAS, one can produce the same energy resolution with an improved spatial resolution

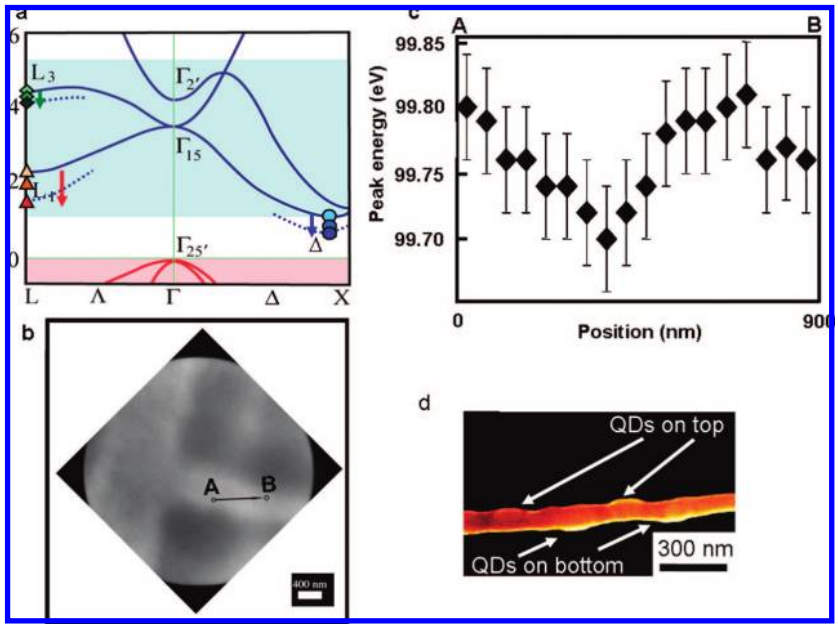

Figure 3. Measurements of the effect of strain on band structure using XAS and PEEM. (a) Schematic diagram of measured results of the shifting of the conduction bands with strain, after ref 19. (b) PEEM image of part of a single Si nanoribbon on which SiGe QDs are grown. (c) Energy of the onset of the XAS 2p-to-Δ transition as a function of lateral position along the arrow in (b). Onset of the transition varies by ~100 meV, with a lateral periodicity of ~350 nm. (d) SEM image of a section of ribbon with SiGe QDs with approximately this periodicity.

of ~50 nm (but with higher noise) (see Supporting Information). We grew SiGe QDs with a lower Ge concentration, so that the stressor QDs are farther apart. Naturally the resulting strain is also lower, so that the variations in band gap are expected to be smaller. Figure 3b shows a PEEM image of part of a single Si nanoribbon on which SiGe QDs are grown. Figure 3c shows the energy of the onset of the XAS 2p-to-Δ transition as a function of lateral position along the arrow in Figure 3b. The onset of the transition varies by ~100 meV, with a lateral periodicity of ~350 nm. Figure 3d shows a SEM image of a section of ribbon with SiGe QDs with approximately this periodicity.

We have therefore demonstrated a band gap modulation along the ribbon created by a periodic strain induced by self-organized nanostressor QDs growing on both sides of the ribbon. This modulation is similar to a 1D heterostructure[23] with essentially all the band offset occurring in the conduction band.[22] The authors of ref 23 calculate the 1D band structure of a superlattice nanowire using a square-well Kronig–Penney model. They demonstrate that the band offset not only provides some amount of quantum confinement but also creates a periodic potential for carriers moving along the wire axis, which may result in a sharper density of electronic states than is present in a normal 1D system, that is, the formation of minibands. In the superlattice nanowire structure, the electronic transport along the wire is by tunneling between adjacent wells. Their results also indicate that the electron band structure is strongly dependent on the period length of the superlattice nanowire (L), the potential barrier heights (V_0), and the transport effective mass (m_e).

A square-well Kronig–Penney model is not realistic for our situation. We have a strain gradient along and through the ribbon. For simplicity, we use a flat-top sinusoidal-like potential shape (Figure 4) in our 1D band structure calculation. We solve the variable-effective-mass Schrödinger equation to obtain the miniband structure in a 1D periodic potential with this potential shape (see Supporting Information). The in-plane electron effective mass is only slightly influenced by strain,[22] and therefore, this factor can be neglected. Increasing the depth of the wells or making them narrower aids in the formation of discrete minibands.

Figure 5 shows our calculated density of states and total number of states for a 1D strain superlattice. When $L_A = L_B = 80$ nm and $V_0 = 250$ meV, corresponding to a pure-Ge QD with a height of 8 nm and a base width of 80 nm grown on a 10 nm thick Si ribbon (Figure 2c), many minibands with very small separations (*i.e.*, minigaps) form within the well, as shown in Figure 5a. We noted that minibands also form above the potential well but are associated with much lower densities of states. The widths of minigaps range from 2 up to 8 meV (Figure 5b), which is much smaller than the thermal energy k_BT at 300 K (~26 meV). These minibands can be essentially considered as continuous states at room temperature (in the classical limit). The Ge/Si nanoribbon structure has to be cooled to below 77 K to minimize the thermal smearing sufficiently to make discrete minibands observable. On the other hand, if the smallest previously observed Ge QD, having a height of 3 nm and a base of 30 nm, is grown on the same thickness Si ribbon, fewer minibands but with larger minigaps form in a shallower potential well ($V_0 = 200$ meV), as shown in Figure 5c. The width of the minigaps (Figure 5d) is about 3-fold larger than that for the conditions represented by Figure 5b. Although this structure still needs to be cooled to observe discrete minibands in the potential well, they would be observable at 77 K. Making the potential wells narrower leads to formation of fewer discrete minibands with larger minigaps. Therefore, each miniband has a higher density of states with less sensitivity to thermal smearing.

Our ultimate goal is to observe discrete minibands in the potential well of the 1D strain superlattice at room temperature because thermoelectric effectiveness of nanowires should be improved.[23] We can, of course, increase the minigaps further by thinning the

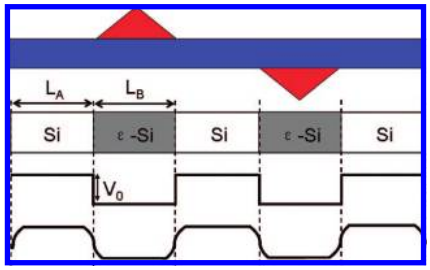

Figure 4. Schematic diagrams of a 1D strain lattice and corresponding periodic-potential shapes, a square well *versus* a flat-top sinusoidal-like well. The latter is used in the calculations.

Si ribbon down to 5 nm (experimentally achievable). A higher strain (1.89%) would be created in Si by the same size of Ge QD, resulting in a deeper potential well (250 meV), leading to an averaged minigap of 15 meV (not shown here). However, such improvements with Ge QDs grown on Si ribbons still cannot make discrete minibands observable at room temperature, no matter how thin the ribbon is.

Strain lattice induced minibands on Si nanoribbons may, however, be accomplished with the use of other nanostressors. For example, it is known that InAs forms nanostressor QDs on Si with a much higher strain (11.5%).[24,25] Our calculations predict that the maximum tensile strain beneath a pure-InAs pyramidal QD with a height of 6 nm and a base width of 11 nm,[25] pseudomorphically grown on a Si membrane, is 1.47% for a 25 nm thick ribbon and 2.68% for a 10 nm thick ribbon. The resulting depression of the band gap is predicted to be up to 350 meV, more than 30% of the bulk value of the band gap for the thinnest ribbons.

Figure 6 shows the calculated density of states and total number of states for a 1D Si strain superlattice created by InAs QDs. We find that well-separated minibands form in the potential well already for a 25 nm thick membrane (potential well depth 200 meV) (Figure 6a), with minigaps ranging from 15 to 85 meV (Figure 6b). In comparison with the Ge QDs grown on Si (Figure 5), the strain from InAs QDs grown on Si creates significantly fewer minibands along with much larger minigaps. Most importantly, Figure 6b shows that only the first minigap is smaller than the thermal energy of ~26 meV at 300 K. It should therefore be possible to observe discrete minibands in the potential near room temperature. Moreover, we can make the potential well deeper (350 meV) by using a 10 nm Si ribbon. The magnitude of minigaps becomes even larger (Figure 6d) as the number of minibands is kept the same (Figure 6c). The first minigap (20 meV) is now comparable to the thermal energy at 300 K, while the rest of the minigaps are almost 100 meV (much larger than 26 meV). It is very important to increase the gaps between the first few minibands, which are associated with very sharp densities of states and are closer to the bottom of the conduction band. It has been shown that the Seebeck coefficient extrema of superlattice nanowires have substantially larger magnitudes if the Fermi energy is near the first few minigaps.[23] We can therefore expect that the Seebeck coefficient of strain-induced electronic superlattices will increase as well, making these types of superlattices promising for thermoelectric applications near room temperature.

In our predictions above, we assume that InAs QDs epitaxially grown on the Si nanoribbon are dislocation free. It is known that, when InAs QDs are epitaxially grown on bulk Si,[24,25] dislocations form at the interface to relax partially the large misfit strain between InAs and Si. As mentioned above, we have demonstrated theoretically[4,11] that strain in Ge QDs is much more effectively transferred to a Si membrane than it is to thick bulk Si. This generic model can be applied to InAs QDs grown Si membrane, as well. The way the strain in the

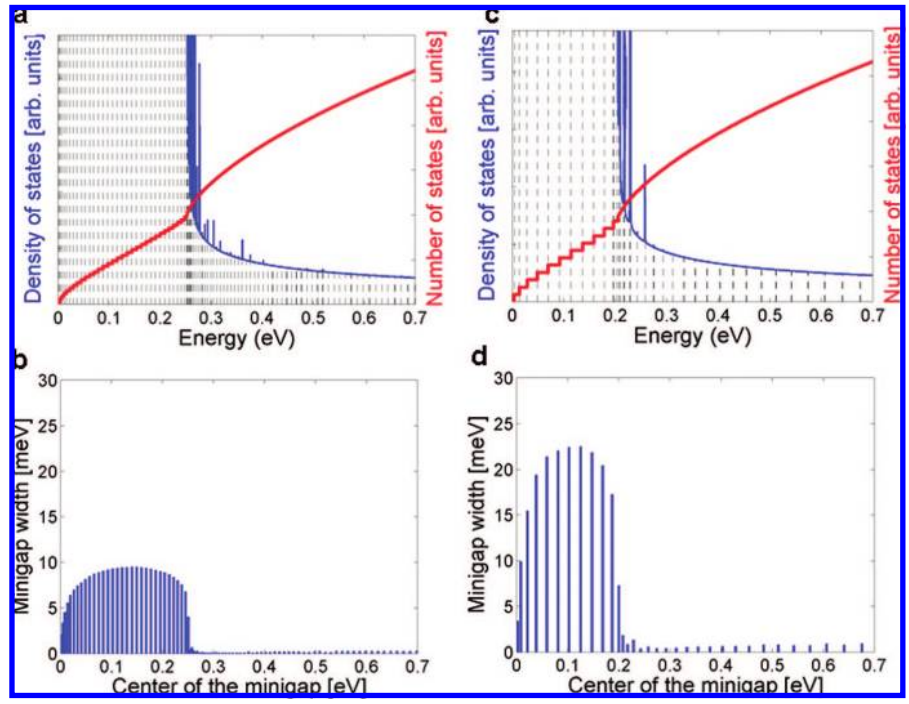

Figure 5. Calculated total number of states (thick red line) and the density of states (thin blue line) for Ge QDs on Si. The reference energy level is the bottom of the quantum well. (a) For potential amplitude $V_0 = 250$ meV, period length $L_A = L_B = 80$ nm, corresponding to ~1.89% strain in 10 nm Si. (b) Minigap width as a function of the energy in the middle of the minigap for the structure in (a). (c) For potential amplitude $V_0 = 200$ meV, period length $L_A = L_B = 30$ nm, corresponding to ~1.53% strain in 10 nm Si. (d) Same as in (b), but for the structure in (c).

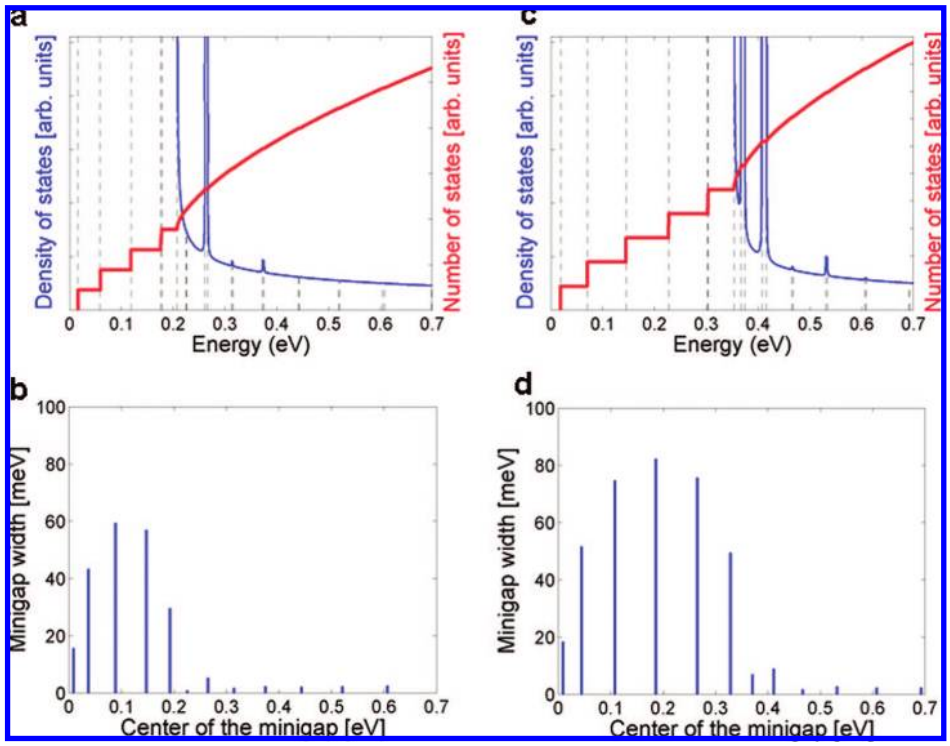

Figure 6. Calculated total number of states (thick red line) and the density of states (thin blue line) for InAs QDs on Si. The reference energy level is the bottom of the quantum well. (a) For a potential amplitude $V_0 = 200$ meV with period length $L_A = L_B = 11$ nm, corresponding to 1.47% strain in 25 nm Si. (b) Minigap width as a function of the energy in the middle of the minigap for the structure in (a). (c) For potential amplitude $V_0 = 350$ meV, period length $L_A = L_B = 11$ nm, corresponding to ~2.68% strain in 10 nm Si. (d) Same as in (b), but for the structure in (c).

InAs QD changes with Si thickness is similar to what occurs in the Ge QD, except for a different magnitude of change. The strain values we use in the InAs calculation are values that are sustainable without dislocation formation. These results will be presented elsewhere.[26]

CONCLUSIONS

In summary, we have demonstrated a way to create electronic superlattices in Si nanoribbons using local, ordered epitaxial nanostressors. The local strain can be made large enough, by using ribbon thicknesses as low as 10 nm and growing nanostressors that produce a high strain, to create band offsets in Si sufficiently large for miniband formation. Under some circumstances, the minigaps may be large enough to observe the minibands at room temperature. The fabrication is easily scalable. Using Si nanomembranes, many identical nanowire or nanoribbon structures with well-defined dimensions can be rapidly created and electrically connected using standard Si processing. Using CVD, growth of QDs on both sides of a nanoribbon occurs; the self-ordering occurs *via* through-membrane elastic interactions.

Electronic superlattices with wells that can result in very sharp densities of states due to the formation of minibands may enhance the Seebeck coefficient, leading to improvements in the thermoelectric figures of merit, if band offsets can be made sufficiently large.[23,27] Combined with recent results demonstrating the effect of Si nanowire size and roughness on improving the thermoelectric figure of merit,[28,29] the introduction of a simple way to modulate the band offsets may be a significant step toward achieving viable near-room-temperature Si thermoelectric nanomaterials. These electronic superlattices may also have unique electron transport properties that may find future device applications.

METHODS

Fabrication of Si Nanomembranes and Nanoribborns. The silicon membranes are fabricated from a SOI wafer that initially has a 200 nm thick Si template layer bonded to a 3 μm thick oxide. Two cycles of thermal oxidation and etching in a 6:1 buffered oxide etching solution remove 90 nm of Si per cycle and leave a Si template layer approximately 25 nm thick. Thinner templates are formed by alternating chemical oxidation in a modified SC1 solution and etching in hydrofluoric acid (HF), removing 2 nm of Si per cycle.[30] The thickness of the template layer is determined with high-resolution X-ray diffraction (XRD) and optical-reflectivity measurements. Electron beam lithography is used to define nanoribbons. By patterning a polymethylmethacrylate resist and then removing the Si template layer in selected areas with reactive ion etching, the exposed underlying SiO_2 can be selectively etched, releasing a Si nanomembrane or a set of nanoribbons.

Growth of Nanostressors. Chemical cleaning prior to chemical vapor deposition (CVD) includes an extended immersion in HF as a final step. The HF exposure removes the sacrificial oxide layer beneath the defined nanoribbons, leaving them free-standing and hydrogen-terminated on both sides. Ge or SiGe QDs are grown by CVD after removal of the H in ultrahigh vacuum.

Instruments and Characterization. XRD measurements were performed on a PANalytical X'Pert PRO diffractometer with high-resolution setup for epitaxial layers (absolute angular resolution = 0.0001 degrees). The electron beam lithography and SEM images were carried out with a LEO DSM 1530 field emission scanning electron microscope. XAS/PEEM measurements were performed at the University of Wisconsin Synchrotron Radiation Center.

Acknowledgment. This work was supported primarily by the U.S. Department of Energy, Office of Basic Energy Sciences, Grant #DE-FG02-03ER46028 and Grant #DE-FG02-03ER46027, and the

National Science Foundation, Award #ECCS-0547415. Added support came from the Air Force Office of Scientific Research, Grant #FA9950-06-1-0472, and by the National Science Foundation through the University of Wisconsin Materials Research Science and Engineering Center. The University of Wisconsin Synchrotron Radiation Center is supported by NSF. We are grateful to K.T. Turner and H.-J. Kim-Lee for sharing the preliminary results of their calculations with us. We would like to thank M. Abrecht and G. Gilbert for help with the PEEM experiments.

Supporting Information Available: Experimental details, including SEM probing of the arrangement of Ge QDs on both sides of a Si nanoribbon, and the strategy of XAS/PEEM measurements. Computational details, including finite-element analysis and 1D band structure calculations. This material is available free of charge *via* the Internet at http://pubs.acs.org.

REFERENCES AND NOTES

1. Hochmuth, R. M.; Evans, C. A.; Wiles, H. C. McCown Mechanical Measurement of Red Cell Membrane Thickness. *Science* **1983**, *220*, 101–102.
2. Huang, J.; Juszkiewicz, M. H.; de Jeu, W.; Cerda, E.; Emrick, T.; Menon, N.; Russell, T. P. Capillary Wrinkling of Floating Thin Polymer Films. *Science* **2007**, *317*, 650–653.
3. Khang, D. Y.; Jiang, H. Q.; Huang, Y.; Rogers, J. A. A Stretchable Form of Single-Crystal Silicon for High-Performance Electronics on Rubber Substrates. *Science* **2006**, *311*, 208–212.
4. Roberts, M. M.; Klein, L. J.; Savage, D. E.; Slinker, K. A.; Friesen, M.; Celler, G.; Eriksson, M. A.; Lagally, M. G. Elastically Relaxed Free-Standing Strained-Silicon Nanomembranes. *Nat. Mater.* **2006**, *5*, 388–393.
5. Yuan, H.-C.; Shin, J. Y.; Qin, G. X.; Sun, L.; Bhattacharya, P.; Lagally, M. G.; Celler, G. K.; Ma, Z. Q. Flexible Photodetectors on Plastic Substrates by Use of Printing Transferred Single-Crystal Germanium Membranes. *Appl. Phys. Lett.* **2009**, *94*, 013102-1−013102-3.
6. Prinz, V. Y.; Seleznev, V. A.; Gutakovsky, A. K.; Chehovskiy, A. V.; Preobrazhenskii, V. V.; Putyato, M. A.; Gavrilova, T. A. Free-Standing and Overgrown InGaAs/GaAs Nanotubes, Nanohelices, and Their Arrays. *Physica E* **2000**, *6*, 828–831.
7. Huang, M.; Boone, C.; Roberts, M. M.; Savage, D. E.; Lagally, M. G.; Shaji, N.; Qin, H.; Blick, R.; Nairn, J. A.; Liu, F. Nanomechanical Architecture of Strained Bilayer Thin Films: From Design Principles to Experimental Fabrication. *Adv. Mater.* **2005**, *17*, 2860–2864.
8. Mo, Y. W.; Savage, D. E.; Swartzentruber, B. S.; Lagally, M. G. Kinetic Pathway in Stranski-Krastanov Growth of Ge on Si(001). *Phys. Rev. Lett.* **1990**, *65*, 1020–1024.
9. Stranski, I. N.; Krastanov, V. L. *Abhandlungen der Mathematisch-Naturwissenschaftlichen Klasse. Sitzungsberichte der Akademie der Wissenschaften in Wien, Math.-naturwiss. Kl. IIb* **1939**, *146*, 797.
10. Kim-Lee, H.-J.; Savage D. E.; Ritz, C. S.; Lagally, M. G.; Turner, K. T. Control of Island Growth with Mechanically Responsive Single-Crystal Nanomembrane Substrates. *Phys. Rev. Lett.* In press.
11. Huang, M.; Rugheimer, P.; Lagally, M. G.; Liu, F. Bending of Nanoscale Ultrathin Substrates by Growth of Strained Thin Films and Islands. *Phys. Rev. B* **2005**, *72*, 085450-1–085450-5.
12. Liu, F.; Rugheimer, P.; Mateeva, E.; Savage, D. E.; Lagally, M. G. Nanomechanics: Response of a Strained Semiconductor Structure. *Nature* **2002**, *416*, 498.
13. Wang, H.; Liu, F.; Lagally, M. G. Directed Self-Assembly of Quantum Dots by Local Chemical Potential Control *via* Strain Engineering on Patterned Substrates. In *Lateral Alignment of Epitaxial Quantum Dots*; Schmidt, O. G., Ed.; Springer Series on Nanoscience and Technology: Berlin; 2007; pp 525−542.
14. Tersoff, J.; Teichert, C.; Lagally, M. G. Self-Organization in Growth of Quantum Dot Superlattices. *Phys. Rev. Lett.* **1996**, *76*, 1675–1678.
15. Springholz, G.; Holy, V.; Pinczolits, M.; Bauer, G. Self-Organized Growth of Three- Dimensional Quantum-Dot Crystals with fcc-Like Stacking and a Tunable Lattice Constant. *Science* **1998**, *282*, 734–737.
16. Jin, G.; Liu, J. L.; Thomas, S. G.; Luo, Y. H.; Nguyen, B.-Y.; Wang, K. L. Controlled Arrangement of Self-Organized Ge Islands on Patterned Si(001) Substrates. *Appl. Phys. Lett.* **1999**, *75*, 2752–2754.
17. Yang, B.; Liu, F.; Lagally, M. G. Local-Strain-Mediated-Chemical-Potential Control of Quantum Dot Self-Organization in Heteroepitaxy. *Phys. Rev. Lett.* **2004**, *92*, 025502-1–025502-4.
18. Ritz, C. S.; Flack, F.; Kelley, M. M.; Savage, D. E.; Detert, D. M.; Evans, P. G.; Cai, Z.; Lagally, M. G. Self-Assembled Structural and Electronic Superlattices On Si Nanoribbons. Unpublished.
19. Euaruksakul, C.; Li, Z. W.; Zheng, F.; Himpsel, F. J.; Ritz, C. S.; Tanto, B.; Savage, D. E.; Liu, X. S.; Lagally, M. G. Influence of Strain on Conduction Band Structure in Strained Silicon Nanomembranes. *Phys. Rev. Lett.* **2008**, *101*, 147403-1–147403-4.
20. Schäffler, F. High-Mobility Si and Ge Structures. *Semicond. Sci. Technol.* **1997**, *12*, 1515–1549.
21. Fischetti, M. V.; Laux, S. E. Band Structure, Deformation Potentials, and Carrier Mobility in Strained Si, Ge, and SiGe Alloys. *J. Appl. Phys.* **1996**, *80*, 2234–2252.
22. Yu, D.; Zhang, Y.; Liu, F. First-Principles Study of Electronic Properties of Biaxially Strained Silicon: Effects on Charge Carrier Mobility. *Phys. Rev. B* **2008**, *78*, 245204-1–245204-8.
23. Lin, Y. M.; Dresselhaus, M. S. Thermoelectric Properties of Superlattice Nanowires. *Phys. Rev. B* **2003**, *68*, 075304-1–075304-14.
24. Mano, T.; Fujioka, H.; Ono, K.; Watanabe, Y.; Oshima, M. InAs Nanocrystal Growth on Si(100). *Appl. Surf. Sci.* **1998**, *130−132*, 760–764.
25. Zhao, Z. M.; Hulko, O.; Yoon, T. S.; Xie, Y. H. Initial Stage of InAs Growth on Si(001) Studied by High-Resolution Transmission Electron Microscopy. *J. Appl. Phys.* **2005**, *98*, 123526-1–123526-4.
26. Huang, M.; Liu, F.; Lagally, M. G. Unpublished.
27. Li, D. Y.; Wu, Y.; Fan, R.; Yang, P. D.; Majumdar, A. Thermal Conductivity of Si/SiGe Superlattice Nanowires. *Appl. Phys. Lett.* **2003**, *83*, 3186–3188.
28. Hochbaum, A. I.; Chen, R.; Delgado, R. D.; Liang, W.; Garnett, E. C.; Najarian, M.; Majumdar, A.; Yang, P. Enhanced Thermoelectric Performance of Rough Silicon Nanowires. *Nature* **2008**, *451*, 163–167.
29. Boukai, A. I.; Bunimovich, Y.; Tahir-Kheli, J.; Uy, J.-K.; Goddard, W. A., III; Heath, J. R. Silicon Nanowires as Efficient Thermoelectric Materials. *Nature* **2008**, *451*, 1168–1171.
30. Celler, G. K.; Barr, D. L.; Rosamilia, J. M. Etching of Silicon by the RCA Standard Clean 1. *Electrochem. Solid State* **2000**, *3*, 47–49.